Analysis of Heat Flow Coupled with Structural Changes in Laser Transformation Hardening Process†

Katsunori INOUE*, Etsuji OHMURA, Nobuo OHATA*** and Yasuyuki TAKAMACHI******

Abstract

Coupling effects between the temperature field and structural changes are considered in the analysis of laser transformation hardening process. The volume fractions of the structural constituents, the latent heat during the phase transformation and structure dependence of the thermophysical properties are introduced during the iterational calculations of the steady-state temperature distribution and the structural changes. The carbon content of a steel, mean value of the grain size of the prior austenite, and the size and the interlamellar spacing of the pearlite colony are input for the initial parameters. Finite-element calculations are carried out to obtain the temperature distribution and the structural changes in the process, and the microhardness distribution in the hardened layer. An example of the numerical computations is shown about a 0.45%C carbon steel. The calculated results are compared with those of the experiments on the laser transformation hardening and found to be in good agreement with them.

KEY WORDS: (Heat Treatment) (Laser Transformation Hardening) (CO_2 Laser) (Finite Element Method) (Heat Conduction) (Phase Transformation) (Kinetics) (Microstructure)

1. Introduction

For the industrial application of the laser transformation hardening, it is useful to be able to estimate beforehand the size and shape of the cross section of the hardened layer, and the distribution of the microstructure and microhardness in it. It is also very important to determine theoretically the optimum conditions of the process for a given application and for a given steel. Ohmura et al.[1] developed a finite-difference computer model to analyze the changes with the time of heat flow, the carbon redistribution in austenite and the subsequent quenching to martensite during laser transformation hardening of hypoeutectoid steel. The analyzed results were shown in the pseudocolor images on the display. The transformation hardening process can be simulated for any given hypoeutectoid steel under any laser irradiating condition. If we can input the initial structure of any hypoeutectoid steel, the computer model can be applied to determine theoretically the best combination of the process variables for the laser transformation hardening in advance.

On the otherhand, it is also required to optimize both the kind of steel and the process variables for the part to be applied of a workpiece. The kind of steel contains the carbon content, grain size of the prior austenite, and so on. Theoretical analysis from the relatively macroscopic view point will be needed to realize this purpose. In this study, the carbon content of a steel, mean value of the grain size of the prior austenite, and the size and the interlamellar spacing of the pearlite colony are input for the initial parameters in the theoretical analysis of laser transformation hardening process. Coupling effects between the temperature field and structural changes are considered in the analysis. The volume fractions of the structural constituents, the latent heat during the phase transformation and structure dependence of the thermophysical properties are introduced during the iterational calculations of the steady-state temperature distribution and the structural changes. Finite element calculations are carried out to obtain the temperature distribution and the structural changes in the process, and the micro-hardness distribution in the hardened layer. An example of the numerical computations is shown about a 0.45%C carbon steel. The calculated results are compared with the experimental results.

2. Analysis of Heat Flow

Shown in **Fig. 1** is a sketch of the transformation hardening process with laser irradiation. The laser beam is stationary while the workpiece moves at a constant velocity v in the x direction. Except during the

† Received on November 5, 1990

* Professor
** Instructor
*** Graduate Student

Transactions of JWRI is published by Welding Research Institute of Osaka University, Ibaraki, Osaka 567, Japan

initial and the final transients of the laser transformation hardening process, the temperature distribution in a workpiece of sufficient length is steady with respect to both the coordinate system and the heat source. Under such conditions, the process is reduced to a steady-state heat flow problem. For a stationary coordinate system, the heat conduction equation including the latent heat due to the phase transformation is giben as

$$\nabla\cdot(\lambda\nabla T)-v\frac{\partial(\rho cT)}{\partial x}+v\sum_{i=1}^{4}(\rho l)_i\left[\frac{\partial\xi}{\partial x}\right]_i=0 \quad (1)$$

where T is the temperature, λ the thermal conductivity, ρ the density, c the specific heat and l the latent heat of the workpiece material. The subscripts 1, 2, 3, and 4 denote the properties and the changes of volume fractions during the A_3 transformation, pearlite dissolution, Bainitic and martensitic transformation, respectively.

The thermophysical properties usually depend on the temperature and are measured at each temperature. It is improper, in the strict sense, to use the data measured in quasi-equilibrium state for the analysis of the laser transformation hardening process without considering the following situations: The phase transformations due to the laser irradiation occur on rapid heating or rapid cooling, therefore the transformation points differ from the temperature given in the equilibrium state diagram, and the transformations do not finish instantly. The thermophysical properties also depend on the metallic structure. The heat affected zone, HAZ caused by the laser transformation hardening consists of vaious structures. For these reasons, a simple postulate on the thermophysical properties of the mixed structures is taken in this study. That is, the thermal conductivity λ and the heat capacity ρc are assumed to be linear conbinations with weight of the volume fractions of the constituents:

$$\lambda=\sum_{k=1}^{6}\xi_k\lambda_k \quad (2)$$

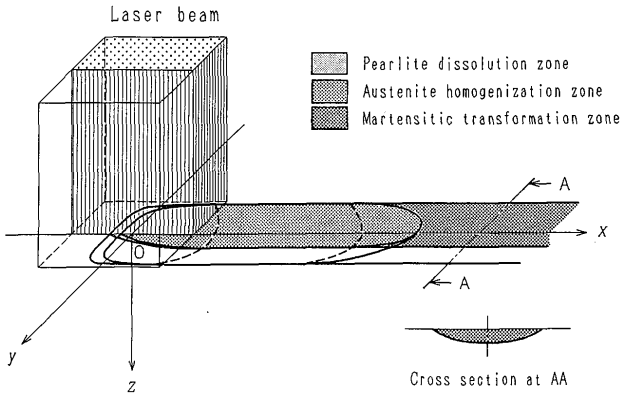

Fig. 1 A schematic sketch of the transformation hardening process with laser irradiation.

$$\rho c=\sum_{k=1}^{6}(\xi_k\rho c)_k \quad (3)$$

where the subscripts 1 to 6 denote the thermophysical properties and the volume fractions of the pearlite, ferrite (α-iron), γ-iron, austenite, fine pearlite and martensite, respectively. Strictly speaking, the thermophysical properties of austenite and martensite also depend on the carbon content.

To solve the heat conduction equation (1), the volume fractions of the constituents should be known, which depend on the heat cycle. The analysis of heat flow must be coupled with the following analysis of structural changes.

3. Analysis of Structural Changes Caused by Heat Cycle

3.1 Dissolution of Pearlite

On rapid heating, the pearlite colonies are transformed to austenite above A_{c1} point. Then carbon diffuses outward from these transformed zones into the surrounding ferrite, increasing the volume fraction of high-carbon austenite. The first process is considered in this section.

The uncleation of austenite in pearlitic structures occurs preferentially at the intersection of pearlite colonies, not at the interlamellar surfaces. The nucleation rate is very large and the nucleation sites would saturate very early in the reaction. Once austenite has nucleated in pearlite, its subsequent growth is presumably controlled by carbon diffusion in the austenite[2]. It is assumed that the changes with time of the volume fraction X of austenite to the matrix, pearlite in the pearlite dissolution is equal to the changes of the volume fraction of pearlite to the matrix, austenite in the pearlite transformation, then the volume fraction X is expressed in the following rate law by Cahn[3]:

$$X=1-\exp(-2SGt) \quad (4)$$

where t is time and S is the boundary area per unit volume. If we assume that a grain of pearlite is a tetrakaidecahedra and the distance between square faces d is the grain size of pearlite, then S is given by

$$S=3.35/d\,. \quad (5)^{3)}$$

And G is the interface velocity; the growth rate of austenite from pearlite, and is given by

$$G=\frac{4}{\pi}\frac{C_\gamma^c-C_\gamma^\alpha}{C_\alpha^\gamma-C_\gamma^\alpha}\frac{D}{l_0} \quad (6)$$

according to Speich et al.[2], where C_γ^α and C_γ^c are the

carbon concentration in the austenite at the midpoint of the α/γ and Fe_3C/γ interface, respectively. C_{α}^{γ} is the concentration in ferrite at the midpoint of α/γ interface. D is the diffusion coefficient of carbon in austenite and l_0 the interlamellar spacing.

In order to apply Eq. (4) in the analysis of the dissolution of pearlite, the continuous heat cycle is divided into a very short time Δt. It is assumed that the isothermal transformation is occured in the time step Δt at the mean temperature, then the volume fraction of the retained pearlite can be calculated by

$$\xi_1 = \xi_1^0\left(1-\sum_{i=1}^{n} X_i\right) \tag{7}$$

where ξ_1^0 is the volume fraction of initial pearlite, n is the number of time step while G is positive, that is, the pearlite dissolusion is progressing. In order to consider that the grain of retained pearlite becomes smaller and smaller with time, the undissolved zone is regarded as a sphere at every time step. The diameter of the sphere d can be calculated with the volume fraction of pearlite at each time, and the boundary area per unit volume S can be obtained by Eq. (5). Then, the volume fraction of austenite X_i during the time Δt is calculated from Eq. (4).

3.2 Homogenization of austenite

Second process in the structural changes during laser transformation hardening is carbon redistribution in austenite, where the carbon diffuses from the high- to the low-concentration regions in an extent which depends on temperature and time. It is postulated that the workpiece consists of concentric spheres, whose diameter $2R_0$ is equal to the mean value of grain size of the prior austenite, of pearlite and ferrite: the former is surrounded by the latter. Then, one dimensional diffusion of carbon is analyzed for the concentric spheres under the newest heat cycle obtained by the iterational calculations of heat flow coupled with structural changes. That is, the modeling for the homogenization of austenite is represented as follows: The spherical particle moves at a constant velocity v along a line parallel to the x-axis, and carbon diffuses in the radial direction under the heat cycle given on the locus of the particle center. It is assumed that the interaction with other moving particles can be ignored. The carbon distribution in the spherical particle which varies with time may be regarded on a average as the carbon distribution at each point on the corresponding line in Fig. 1.

Fick's laws permit the concentration of carbon to be determined as a function of distance and time. The difference equation, the boundary conditions, and the initial conditions in this model are given as follows:

$$\frac{\partial C}{\partial t} = \frac{1}{r^2}\frac{\partial}{\partial r}\left[r^2 D\frac{\partial C}{\partial r}\right] \tag{8}$$

$$\frac{\partial C}{\partial r}(0, t) = 0\,, \quad \frac{\partial C}{\partial r}(R_0, t) = 0 \tag{9}$$

$$\left.\begin{aligned} C(r, 0) &= 0.77 \qquad 0 \leqq r \leqq R_p \\ C(r, 0) &= 0.0218, \quad R_p < r \leq R_0 \end{aligned}\right\} \tag{10}$$

where $2R_p$ is the mean value of the diameter of pearlite colonies. The diffusion coefficient of carbon D depends on both temperature and carbon concentration, and is given by

$$D = D_0(C)\exp\left[-\frac{Q(C)}{RT}\right] \tag{11}$$

where D_0 is the frequency factor, Q the activation energy and R the gas constant, 8.314 J/(mol·K). D_0 and Q depend on both temperature and carbon concentration, and can be expressed by the following equations, which are obtained by a least squares method using the data given by Wells et al.[4].

$$D_0 = 51.568\exp(-1.471C) \qquad [mm^2/s] \tag{12}$$

$$Q = -4.91C^2 - 19.59C + 154.35 \quad [kJ/mol]. \tag{13}$$

The volume fraction of ferrite ξ_2 is obtained as the ratio of the volume of the zone remained to be 0.0218 wt%C, which is given by solving Eqs. (8) to (10), to the volume of whole shpere. The volume fraction of austenite ξ_4 can be estimated by

$$\xi_4 = 1-(\xi_1+\xi_2) \tag{14}$$

where ξ_1 is given by Eq. (7).

Both the α-γ transformation on heating and the γ-α transformation on quenching is assumed to be caused by a massive transformation mechanism.

3.3 Martensitic transformation

On subsequent cooling, austenite is transformed to martensite or fine pearlite, if the cooling rate is higher than the critical cooling rate or not, respectively. The critical cooling rate depends on the carbon content: It decreases with carbon content and is constant above eutectoid content[5]. This curve is approximated by a poligonal line and the results can be used in the present analysis. The cooling rate is calculated at 973 K[6] and is compared with the critical cooling rate. Fine pearlite

is assumed to be obtained at the B_s point, which is given by

$$B_s(K) = 1083-270C-90Mn-37Ni-70Cr-83Mo \quad (15)^{7)}$$

and its dependence on carbon concentration is considered. Fine pearlite obtained in laser transformation hardening is usually very little. It can be postulated that the transformation of fine pearlite from austenite occurs instantaneously, and the kinetic equation is not considered. Therefore, the volume fraction of fine pearlite ξ_5 is governed by the carbon concentration obtained in the carbon diffusion analysis, the B_s point and the cooling rate.

The temperature at which austenite starts to be transformed to martensite, that is, the M_s point also depends on the composite of the austenite, and is given by

$$M_s(K) = 812-432C-30.4Mn-17.7Ni-12.1Cr-7.5Mo. \quad (16)^{8)}$$

Below the M_s point, it is assumed that the retained austenite is transformed to martensite according to the equation[9]:

$$X = 1-\exp[-0.0206\,(M_s-T)^{0.93}], \quad (17)$$

where X is the volume fraction of martensite to the matrix of austenite with 0.50 wt%C. The carbon concentration of martensite obtained in laser transformation hardening can be regarded on a average as about 0.5 wt%C, because the carbon distribution is not uniform. In the present analysis, the martensitic transformation depends on the M_s point and temperature, but the numerical values in Eq. (17) are constant regardless of the carbon concentration. The volume fraction of martensite with carbon concentration C is given by

$$\xi_0(C) = \xi_4^0(C)X(C) \quad (18)$$

where $\xi_4^0(C)$ is the volume fraction of austenite whose carbon concentration is C just before the martensitic transformation starts, and satisfys the following equaion:

$$\int \xi_4^0(C)dC = 1-(\xi_1+\xi_2+\xi_5). \quad (19)$$

Through above analysis, we can obtain the volume fractions of pearlite, ferrite (α-iron), γ-iron, austenite, fine pearlite and martensite, and the carbon distribution at each point in the structural-changing zone in Fig. 1. The latent heat caused by transformations are obtained by the third term in Eq. (1); the thermophysical properties are obtained by Eqs. (2) and (3). The heat flow is analyzed again with these results, then the structural changes are anlyzed again. The iterational calculations are continued until the temperature distribution converges. The outline of the procedure in analysis is shown in **Fig.2.**

The hardness distribution of the HAZ depends on the volume fractions of constituents and carbon concentration. Using the results obtained through above analysis, the hardness distribution can be calculated by summarizing the hardness H of each constituent with weight of the volume fraction, as follws:

$$H_v = H_1\xi_1+H_2\xi_2+H_4\xi_4+H_5\xi_5+\int H_6(C)\xi_6(C)dC \quad (20)$$

where the 5th term shows that the carbon-concentration dependence of hardness for martensite is considered and the hardness is calculated by summarizing hardness related to the carbon concentration with weight of the volume fraction of martensite which contains the carbon concentration.

4. Laser Transformation Hardening Experiments

The transformation hardening was carried out using a continuous wave CO_2 laser developed by GTE SYLVANIA Co. The maximum power capacity was

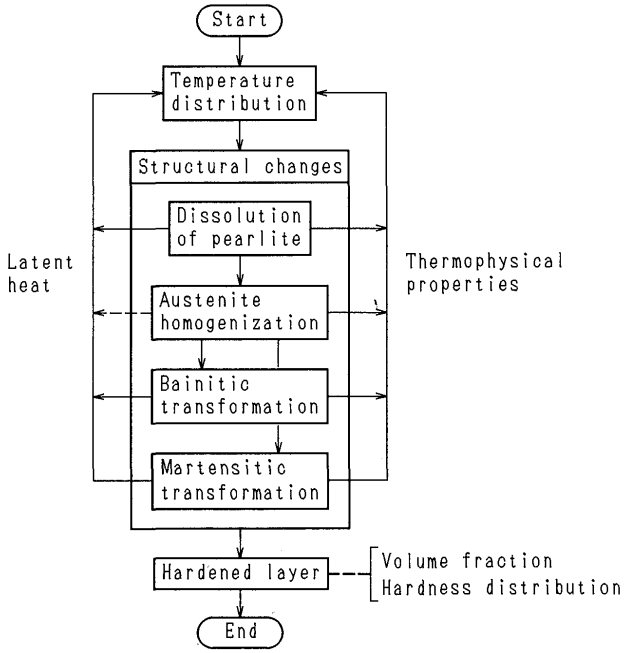

Fig. 2 Procedure of analysis.

5 kW. An integration mirror and a Zn-Se lens were used to generate a square laser beam of uniform energy distribution.

The workpiece used was 100 mm long, 50 mm wide, and 10 mm thick, and the work material was normalized carbon steel S45C which was equivalent to AISI 1045. The chemical composition of the material is shown in **Table 1**. The top surface of the workpiece was machined smooth, and coated with carbon in order to enhance the surface absorptivity. The laser irradiating condition is shown in **Table 2**.

After the laser irradiation, the workpiece was sectioned transverse to the direction of travel, polished, and etched with 5 pct. Nital. The microstructure of the heat-affected zone was examined by a metallographic microscope. The hardness distribution of this sample was measured with micro-Vickers hardness tester at a load of 2.94 N. The workpiece was also sectioned in parallel to the direction of travel, and the volume fractions of the retained pearlite and ferrite were measured at each depth. The method was as followed: The length which pearlite or ferrite occupy in the photograh of microstructure was measured along the line of 5 mm long on the sample, and the volume fractions ξ_1 and ξ_2 of pearlite and ferrite, respectively, were given as the ratio of the sum of length of each constituent to the total length, 5 mm.

Before the irradiation experiments, the particle area of pearlite in the base metal was measured by the image processing technique, and the mean value of the diameter of pearlite was calculated using Johnson-Saltykov method[10]. The mean number of grains of which the pearlite colonies consist was observed through a microscope, and the interlamella spacing was measured using SEM.

5. Numerical Computation Methods

Finite element method is used for the numerical computations in this study. Since the heat flow is symmetrical with respect to the O-xz plane, only one half of the workpiece is considered in analysis. The heat loss from O-xy plane was neglected[1]. The computational domain was -4.2 mm to 14.7 mm for the x direction, 0 to 8 mm for both y and z directions, respectively. The x-, y- and z-directions of this domain were divided into 44, 9 and 10, respectively. A small rectangular-parallelepiped caused by the division is called block in this paper. Considering that the temperature varies drastically near the heat source and slightly at other area, the blocks were kept small where high temperature gradients were expected. Each block was divided into six tetrahedrons. Four-nodes linear elements were adopted and Eq. (1) was reformed in the discrete form with Galerkin method. The coefficient matrix of the linear equations is an asymmetric band matrix, and varies with iteration. Therefore, Gauss elimination method considering a band matrix was adopted for the numerical computation of the linear equations.

The initial temperature was given to be 293 K and the structure dependence of the thermophysical properties and the latent heat during the transformation were considered as above mentioned. The data[11-14] used for the computation of the thermal conductivity, thermal diffusivity and density are shown in **Table 3**. The latent heat used is shown in **Table 4**. The thermophysical properties of the austenite and martensite in hypoeutectoid steel depend on the carbon content, districtly, but the relative difference is blow 10 pct, therefore, the measured value for 0.42W%C. which is the mean value for hypoeutectoid steel, was adopted in the present computations.

The mean value of the diameter of pearlite colonies $2R_P$ was given to be 35 μm according to the experimental result (see section 4). Four or six grains were observed mainly in a pearlite colony through the microscope, it was postulated that one pearlite colony consists

Table 1 Chemical composition of material used.

C	Si	Mn	P	S	Cu	Ni	Cr
0.436	0.25	0.71	0.017	0.016	0.13	0.06	0.12

Table 2 Laser irradiating conditions.

Laser power	1.14kW
Beam size	4.4mmX4.4mm
Traveling velocity	30mm/s

Table 3 Thermal conductivity, thermal diffusivity and density used for calculations.

	λ W/(m·K)	a mm^2/s	ρ kg/m^3
Ferrite	48.4	9.34	7.87X10^3
Pearlite	39.3	8.83	7.85X10^3
Austenite	28.2	6.52	8.15X10^3
Fine pearlite	39.3	8.83	7.85X10^3
Martensite	42.0	1.19	7.80X10^3

Table 4 Latent heat used for calculations.

Dissolution of pearlite	20.9kJ/kg
A_3 transformation	16.5kJ/kg
Bainitic transformation	20.9kJ/kg
Martensitic transformation	75.3kJ/kg

of eight grains as mean value. Then the average diameter d of one grain is 17.5 μm. The interlamella spacing was given to be 2500 Å through SEM observation.

In the numerical computation of the pearlite dissolution and the homogenization of austenite, each block in the analysis of heat flow was divided into 125 rectangular-parallelpipeds, which are called units in this study, by dividing each edge of one block into five. A_{c1} spherical particle, which consists of pearlite and ferrite, moves along the center line of a row of units parallel to the x-axis, and has the heat cycle given on the center line. In the spherical particle, pearlite is surrounded concentrically by ferrite, and the diameter of particle $2R_0$ is 43 μm in this case (see section 3.2).

After the temperature of spherical particle reached A_{c1} point, the volume fraction of retained pearlite at the center of each boundary perpendicular to the x-axis of units was calculated by Eq. (7), and the latent heat generated at the center of unit was calculated by the third term of Eq. (1). The amount of heat obtained was distributed to eight nodes of the block to which the unit belonged, considering the distance between the center of the unit and each node of the block. The distance was elminated by the volume of eight rectangular-parallelpipeds which were supposed to divide the block. The amount of heat distributed was substituted into the heat flux vector in the analysis of heat flow. Then the carbon distribution at the center of each boundary perpendicular to the x-axis of units was calculated through Eqs. (8) to (10) under the present heat cycle, using the finite element technique. The r-axis of the spherical particle was divided into 150 with linear-elements.

On subsequent cooling, B_s and M_s points at every time for each node in the analysis of carbon diffusion was calculated, substituting the carbon concentration obtained into Eqs. (15) and (16), continuously. When the temperature at the boundary of the units reachs B_s or M_s points, austenite is transformed to martensite or fine pearlite, if the cooling rate is higher than the critical cooling rate or not. If the transformation was martensitic, the volume fraction of martensite for each node was calculated by Eq. (18), and the total volume fraction ξ_6 at the boundary surface of the unit perpendicular to x-axis was obtained by summarizing the volume fractions of all nodes in the analysis of carbon diffusion. The latent heat generated was calculated by the third term of Eq. (1), as well as the pearlite dissolution. The amount of heat was distributed to eight nodes of the block to which the unit belonged, then was substituted into the heat flux vector. The transformation of fine pearlite was assumed to be instantaneously, above mentioned.

In the analysis of the hardness distribution, the data used for the Vickers hardness of ferrite, fine pearlite and retained austenite were 95, 480 and 187, respectively. The hardness of pearlite is given as a function of the interlamellar spacing l, therefore, Hv=315 was adopted as l was 2500 Å in this study. On the carbon-content dependence of the hardness of martensite, we related the hardness of martensite to its mean carbon content by fitting a quadratic expression to the data between 0 and 0.77 wt%C compiled by Leslie[15].

6. Results and Discussion

Analyses of heat flow and structural changes in the workpiece during transformation hardening under the laser irradiating condition shown in Table 2 were carried out based on the theory discussed in the previous sections.

Figure 3 shows the temperature distribution in the workpiece. The absorptivity was assumed to be constant in the heat flow calculation. By using 1063 K[16] as the effective A_{c1} point on heating, the size of the HAZ was calculated. An absorptivity of 75.9 pct was found

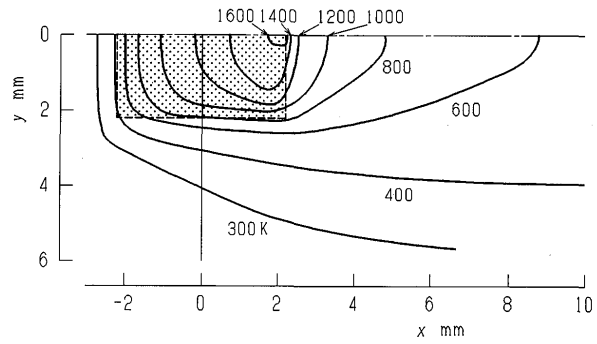

(a) O-xy plane.

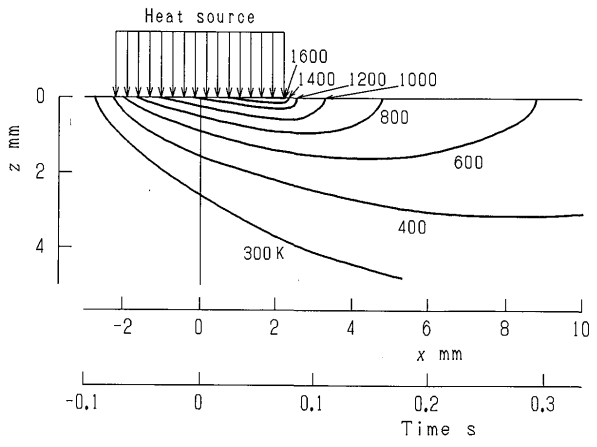

(b) O-xz plane.

Fig. 3 Temperature distribution.

to fit best both the depth and the width of the HAZ observed.

The broken lines in Fig. 3 (a) show the shape of the heat source. The maximum temperature at the workpiece surface is near the end edge, rather than at the center, of the rectangular heat source. The time scale in this figure is used to show the structural changes, as will be shown later. Time zero corresponds to the center of the heat source. The cooling rate is relatively greater than the heating rate. The cooling rate at 973 K is faster at the both sides than at the central area of the HAZ, as shown in **Fig. 4**.

Figure 5 shows the process of the structural changes in the O-xz plane of the workpiece with time, which corresponds to the position of the x direction in Fig. 3. The depth of this hardened layer is about 470 μm. The pearlite dissolution does not start when the front edge of the laser beam reachs, but starts when 1/4 or 1/3 of the beam passes. The dissolution of pearlite finish first near the heat source as the heating rate is largest, and the time used is about 10 ms. The pearlite retains slightly above the boundary of the hardened layer without sufficient dissolution.

Self-quenching occurs progressly from the surface to the interior area. The carbon atoms scarcely diffuse on rapid cooling, because the diffusion coefficient of carbon in austenite becomes small rapidly since the temperature decreases at a high cooling rate. The

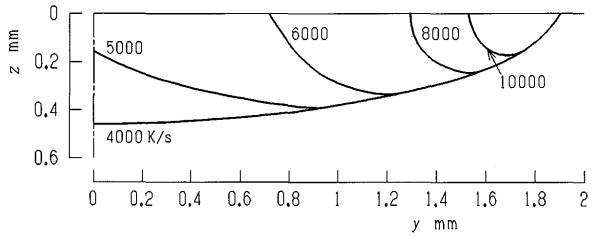

Fig. 4 Distribution of the cooling rate at 973 K.

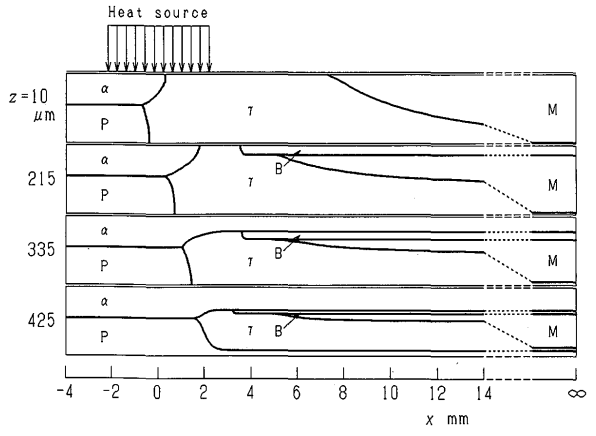

Fig. 5 Structural changing process in O-xz plane, where P is pearlite, α ferrite, γ austenite, B fine pearlite and M martensite.

distribution of the carbon concentration in the hardened layer is determined neat x=3 mm.

The final carbon distribution at each depth in Fig. 5 is shown in **Fig. 6**. Fine pearlite appears from the deepest part of the HAZ where the carbon atoms diffuse slightly, because the B_s point becomes higher as the carbon concentration is lower (see Fig. 5). The fine pearlite can not be found at the surface area, as the carbon atoms diffuse sufficiently and the cooling rate is higher. Slightly above the boundary of the HAZ, the pearlite colonies are transformed to austenite without sufficient diffusion of carbon into the surrounding ferrite. Therefore, the carbon concentration of the martensite is almost 0.77 wt%C, which is the same value as pearlite (see Fig. 6).

The volume fractions of the final structure in the y-z plane are shown in **Fig. 7** (a) to (d). The structure distribution in the hardened layer depends on the shape of the HAZ, especially the distribution of the maximum temperature reached. For the reason of that time held above A_{c1} point is relatively long in the both side of the hardened layer, as shown in Fig. 3, and the cooling rate at the area is higher than that at the center of the boundary of HAZ (see Fig. 4), fine pearlite is not appeared in the area. The hardness distribution estimated for this hardened layer is shown in **Fig. 8**, which also depends on the maximum temperature reached.

The microstructure of the HAZ obtained by the experiment is shown in **Fig. 9**, and the shape of the cross section of the hardened layer and the distribution of the structure are found to be in good agreement with the estimated results on the first inspection. In order to estimate the validity of the calculated results more quantatively, the volume fractions of the pearlite and ferrite, ξ_1 and ξ_2 in the two x-z planes contain A-A′ and B-B′ in Fig. 9 were measured. It was confirmed in the previous study[17] that there are fine pearlite and retained austenite in the hardened layers obtained by laser transformation hardening, but it is difficult to estimate quantitatively the volume fractions of them,

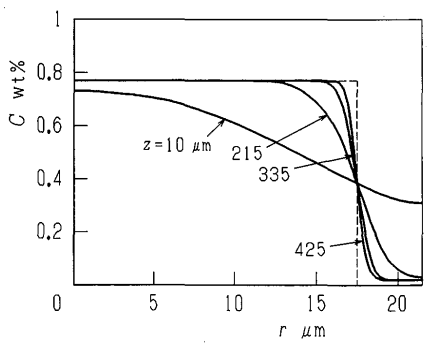

Fig. 6 Distribution of carbon concentration at each depth of Fig. 5.

therefore it is not easy to measure the volume fraction of martensite which contains them. For this reason, the volume fractions of retained pearlite and ferrite were measured in this study. The results are shown in **Fig. 10**, in which the volume fraction of ferrite and the sum of the volume fractions of matrensite, fine pearlite and retained austenite, which is estimated by $1-\xi_1-\xi_2$. The calculated results on the volume fraction of martensite are also shown in Fig. 10. The estimated results are in fairly good areement with the experimental results.

Figure 11 shows the hardness distribution of the cross section of the HAZ obtained by the experiment and the estimation. The measurements were carried out from the surface to the depth along the central axis and two lines whose distances were 50 μm on both sides from the central axis, in the two cross sections, respectively. The estimation was done at the same places. We find that agreement is satisfactory.

These analytical results are shown to be in good

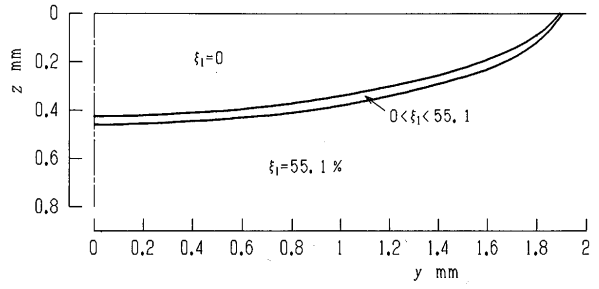

(a) Martensite.

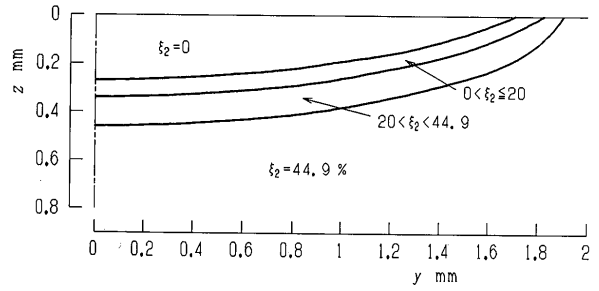

(b) Ferrite.

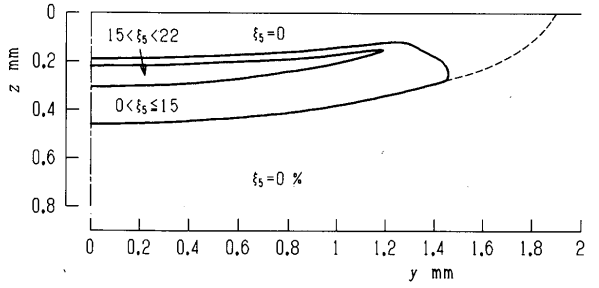

(c) Fine pearlite.

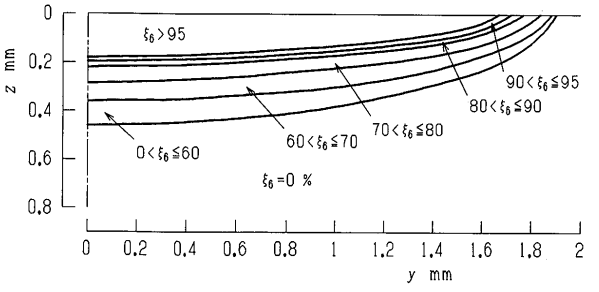

(d) Martensite.

Fig. 7 Volume fractions of structural constituents in the hadened layer.

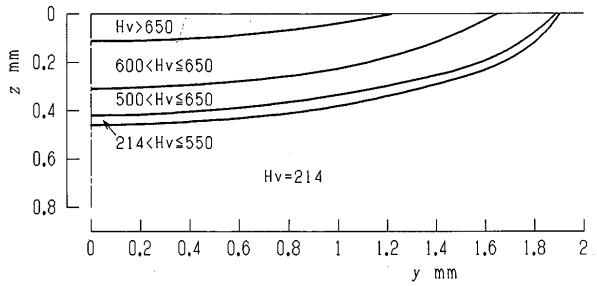

Fig. 8 Hardness distribution in the hardened layer.

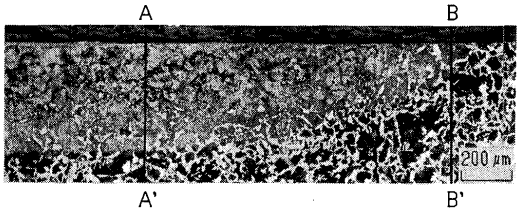

Fig. 9 Microstructure of the hardened layer.

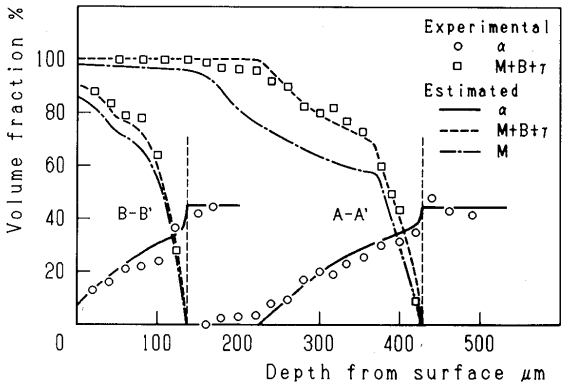

Fig. 10 Distribution of structural constituents in the two *x-z* planes contain A-A′ or B-B′ shown in Fig. 9.

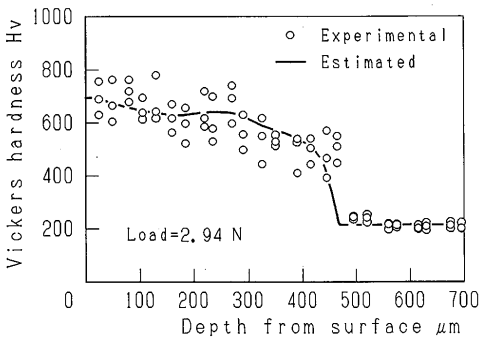

Fig. 11 Hardness distribution obtained by the experiment and the estimation near the central axis in the HAZ.

agreement with the experimental results, thus indicating that the method of analysis proposed in this study is fully acceptable.

7. Conclusion

It is important for the industrial application of the laser transformation hardening to optimize not only the process variables but also the kind of steel for the part to be applied of a workpiece. Theoretical analysis from the relatively macroscopic view point will be needed to realize this purpose. In this study, the carbon content of a steel, mean value of the grain size of the prior austenite, and the size and the interlamellar spacing of the pearlite colony are input for the initial parameters in the theoretical analysis of laser transformation hardening process. Coupling effects between the temperature field and structural changes are considered in the analysis. Finite-element calculations were carried out to obtain the temperature distribution and the structural changes in the process, and the microhardness distribution in the hardened layer. An example of the numerical computations was shown about a 0.45 wt%C carbon steel. The calculated results were verified experimentally and found to be in good agreement with them.

The theory proposed in this study can be applied to determine theoretically the best combination of the process variables and the appropriate kind of steel for the laser transformation hardening in advance.

Acknowledgement

This research was supported in part by Grant-in-Aid for Scientific Research from the Ministry of Education, Science and Culture of Japan.

References

1) Ohmura, E., Inoue, K. and Haruta, K., Computer Simulation on Structural Changes of Hypoeutectoid Steel in Laser Transformation Hardening Process, *JSME Int. J.*, Vol. 32 (1989), p. 45.
2) Speich, G.R. and Szirmae, A., Formation of Austenite from Ferrite and Ferrite-Carbide Aggregates, *Tarns. Metall. Soc. AIME*, Vol. 245 (1969), p. 1063.
3) Cahn, J.W., The Kinetics of Grain Boundary Nucleated Reactions, *ACTA Met.*, Vol. 4 (1956), p. 449.
4) Wells, C., Batz, W. and Mehl, R.F., Diffusion Coefficient of Carbon in Austenite, *Trans.AIME*, Vol. 188 (1950), p. 553.
5) Suzuki, H., *Handbook of Welding*, (in Japanese), (1977), p. 227, Sankaido.
6) Ohwaku, S., *Handbook of Heat Treatment for Metals and Alloys*, (in Japanese), (1966), p. 195, Nikkan-Kogyo-Shinbunsha.
7) Steven, W. and Haynes, A.G., The Temperature of Formation of Martensite and Bainite in Low-Alloy Steels, *J. Iron Steel Inst.*, Vol. 183, (1956), p. 349.
8) Andrews, K.W., Empirical Formulae for the Calculation of the Transformation Temperature, *J. Iron & Steel Inst.*, Vol. 203 (1965), p. 721.
9) Hougardy, H.P. and Yamazaki, K., An Improved Calculation of the Transformation of Steels, *Steel Research*, Vol. 57 (1986), p. 7.
10) DeHoff, R.T. and Rhine, F.N., *Quantitative Microscopy*, (1968), McGraw-Hill.
11) *Metals Handbook*, 9th ed., Vol. 1 (1978), p. 145, ASM.
12) ibid, Vol. 2 (1979), p. 741 ASM.
13) Wang, Z.G. and Inoue, T., Analyses of Temperature, Structure and Stress during Quenching of Steel with Consideration for Stress Dependence of Transformation Kinetics, *J. Soc. Material Science* (in Japanese), Vol. 32, No 360, (1983), p. 991.
14) *Metal Data Book*, 2nd ed., (in Japanese), (1984), p. 84, Maruzen.
15) Leslie, W.C., *The Physical Metallurgy of Steels*, (1981), McGraw-Hill.
16) Orlich, J., Rose, A. and Wiest, P., *Atlas Zur Wärmebehandlung der Stähle*, Vol. 3 (1977), p. 79.
17) Ohmura, E. and Namba, Y., Microstructure of Hypo-Eutectoid Steel in Laser Hardening Process, *Trans. Jpn Soc. Mech. Eng.*, (in Japanese), Vol. 51, No. 469, A (1985), p. 2231.